Journal of Photochemistry and Photobiology A: Chemistry 220 (2011) 85–93

Contents lists available at ScienceDirect

Journal of Photochemistry and Photobiology A: Chemistry

journal homepage: www.elsevier.com/locate/jphotochem

Role of TiO_2 surface hydration on NO oxidation photo-activity

Andrea Folli*, Steven B. Campbell, James A. Anderson, Donald E. Macphee*

Department of Chemistry, University of Aberdeen, Meston Walk, AB24 3UE Aberdeen, UK

ARTICLE INFO

Article history:
Received 21 November 2010
Received in revised form 16 March 2011
Accepted 20 March 2011
Available online 1 April 2011

Keywords:
TiO_2
Nitric oxide
Nitrate
Surface hydration
Photoadsorption
Photocatalytic oxidation

ABSTRACT

The paper highlights the role of TiO_2 surface hydration in the conversion of nitric oxide, NO, under irradiation of UVA light. H_2O desorption thermokinetics of TiO_2 surface is studied to characterise the state of water on TiO_2 and identify criteria for potential thermal dehydration. Hydrated and dehydrated surfaces are then studied for their ability to oxidise gaseous NO and emphasise the overall role of H_2O_{ads} and OH_{ads} groups and the differences between initial and transient regimes before reaching steady state. A model based on a rapid initial NO reactive *photoadsorption* is used to interpret the high initial removal of NO which develops in a lower NO conversion transient regime. The development of NO and NO_2 profiles as a function of time coupled with the total NOx balance in the gas phase, also offer ways to understand deactivation phenomena at the catalyst surface.

1. Introduction

Nitrogen oxides (NOx) air pollution is an important issue facing modern societies. Mainly responsible for *photochemical smog* [1] (a mixture of hazardous chemicals derived from the interaction of sunlight with atmospheric pollutants); NOx together with sulphur oxides (SOx) generate acid rains [1–3] and by direct exposure, or from acid vapours arising from their interaction with atmospheric moisture, can cause emphysemas and bronchitis [1]. Further, they can seriously affect regular metabolic processes in plants [1]. NOx refers to the sum of NO and NO_2. NO is directly introduced into the atmosphere from a source (e.g. high temperature combustion in transport and industry [1–4]). NO_2 is formed into the atmosphere by reaction between NO and ozone, O_3, or molecular oxygen (even though the reaction with the latter is kinetically slow) assisted by sunlight [1–4]. Further reactions in the atmosphere can transform NO and NO_2 into nitric acid, HNO_3, peroxyacyl nitrates (PANs), $RC(O)OONO_2$, peroxynitric acid, HNO_4, etc. The sum of all these species and NOx is known as NOy, *reactive nitrogen compounds*.

The control and remediation of atmospheric NOx has been largely driven by environmental legislation. The prevention and remediation technologies for NOx, include combustion modifications, dry and wet processes [5–7]. Photocatalytic oxidation (PCO) of NOx using titanium dioxide as semiconductor photocatalyst has become, over the past ten years, a competitive alternative, as confirmed by the growing number of commercial products available on the market and the increasing scientific focus [8–19]. PCO has the great advantage that the only requirements for functionality are sunlight (containing 7–8% of UV light necessary for the activation of TiO_2), atmospheric oxygen and water, which means that remediation is continuous in daylight.

The photocatalytic mechanism is dependent on the semiconductor properties of TiO_2. Under illumination with UV light, conductance band electrons and valence band positive holes are generated which react with oxygen and water, respectively, on the catalyst surface to form a range of oxygen-based radicals [14,20], according to Eqs. (1)–(7):

$$3H_2O + 3h^+ \leftrightarrow 3HO^\bullet + 3H^+ \quad (1)$$

$$2O_2 + 2e^- \leftrightarrow 2O_2{}^{-\bullet} \quad (2)$$

$$O_2{}^{-\bullet} + H^+ \leftrightarrow HO_2{}^\bullet \quad (3)$$

$$HO_2{}^\bullet + e^- \leftrightarrow HO_2{}^- \quad (4)$$

$$HO_2{}^- + H^+ \leftrightarrow H_2O_2 \quad (5)$$

$$O_2{}^{-\bullet} + H_2O_2 \leftrightarrow OH^- + HO^\bullet + O_2 \quad (6)$$

$$H^+ + OH^- \leftrightarrow H_2O \quad (7)$$

which correspond to the overall reaction:

$$H_2O + \frac{1}{2}O_2 \leftrightarrow 2HO^\bullet \quad (8)$$

Devahasdin et al. [12] studied the oxidation mechanism of NO on TiO_2 in a continuous reactor fed with a mixture of NO, air and H_2O. The proposed reaction mechanism is rather complex and involves

* Corresponding authors.
E-mail addresses: a.folli@abdn.ac.uk (A. Folli), d.e.macphee@abdn.ac.uk (D.E. Macphee).

1010-6030/$ – see front matter © 2011 Elsevier B.V. All rights reserved.
doi:10.1016/j.jphotochem.2011.03.017

Table 1
TiO_2 physical characterisation data.

Sample	Crystalline Phase	Band Gap	SBET	BJH Φ_{pore}	Particle size		
					TEM	XRD	BET
		eV	m^2g^{-1}	Å	nm	nm	nm
n-TiO_2	100% Anatase	3.34 ± 0.02	78.9	79.6	18.4 ± 5.0	16.6 ± 2.0	19.5

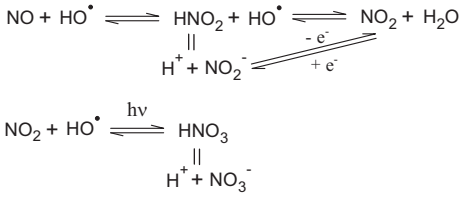

Fig. 1. Reaction networks for photocatalytic oxidation of nitric oxide over TiO_2.

a long series of reactions where, on the TiO_2 surface, adsorbed NO reacts with adsorbed •OH forming nitric acid, HNO_3, passing through two intermediates: unstable nitrous acid, HONO, and nitrogen dioxide, NO_2. This series of reactions can be summarized through the simplified reaction network shown in Fig. 1 [12].

The availability of water in PCO of NO is a crucial factor. Devahasdin et al. [12] demonstrated that the lower the water vapour pressure in the system (controlled through the relative humidity of the gas stream) the lower the NO conversion. In this paper we investigate the role of water in more detail examining the state of water on the TiO_2 surface and correlating the effect of surface dehydration, for a fixed O_2 partial pressure, to NO conversions and on the synergistic role of the H_2O/O_2 couple in the photocatalytic oxidation process of NO. N mass balance data are here also used to identify possible deactivation mechanisms.

2. Materials and methods

2.1. TiO_2 sample

The photocatalyst used throughout the experiment is a nano-sized 100% anatase TiO_2 (n-TiO_2) studied and fully characterised elsewhere [21]. Table 1 summarizes the main physical-chemical properties of the sample.

2.2. Thermokinetics of TiO_2 surface dehydration

Diffuse reflectance infrared Fourier transform Spectra (DRIFT) have been collected over the temperature range 25–500 °C (heating rate 5.0 °C min^{-1}) using a Perkin Elmer Spectrum 100 with a diffuse reflectance cell equipped with an electrical heating system. Spectra were processed using the associated software. Thermo-gravimetric (TG) data were obtained using a Stanton STA 780 vertical thermo balance analyser interfaced with a personal computer through a Pico Data Collector and Pico Data Recorder software. The temperature range scanned was 25–1000 °C (5.0 °C min^{-1}).

2.3. TiO_2 coated glass beads preparation

Glass beads (Sigma–Aldrich; diameter 450–600 μm) were coated with n-TiO_2 by the method of Daneshvar et al. [22] (Fig. 2) and used as a photocatalytic bed in the NO oxidation experiment. 3 g of n-TiO_2 were dispersed in 200 ml of deionised water and sonicated in an ultrasonic bath for 15 min to achieve good dispersion of titania particles. 30 g of glass beads (without any pre-treatment) was added to the dispersion and left to stand for a further 15 min under sonication. The beads were then filtered on a Buchner filter,

Fig. 2. SEM micrograph of a n-TiO_2 coated glass bead.

placed in oven at 106 °C for 3 h and when dry, fired at 500 °C for 1 h. After firing the coated beads were placed in a column fitted with a porous disc, washed by flushing 200 ml of deionised water, placed again on a Buchner filter and washed with an excess of deionised water. The final step consisted in a further drying at 106 °C for 30 min. Once dry, the TiO_2 coated glass beads were stored in a light-tight jar at room temperature under ambient air conditions. The amount of TiO_2 deposited was 0.11 $g_{TiO_2}\, g^{-1}_{glassbeads}$ B.E.T. specific surface area of coated glass beads has been previously measured by N_2 adsorption using a Micromeritics ASAP 2020. SEM micrographs of coated glass beads have been obtained using a Hitachi S-520 Scanning Electron Microscope.

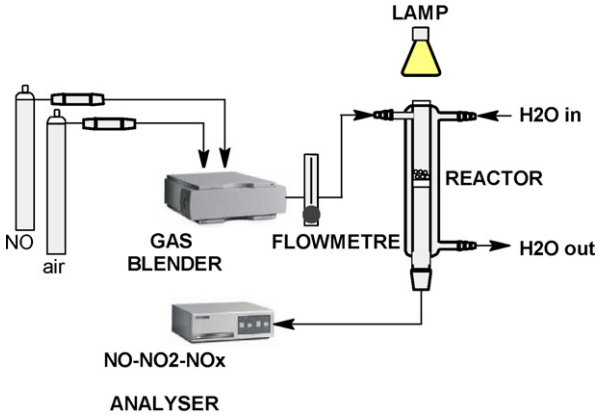

Fig. 3. NO oxidation lab plant.

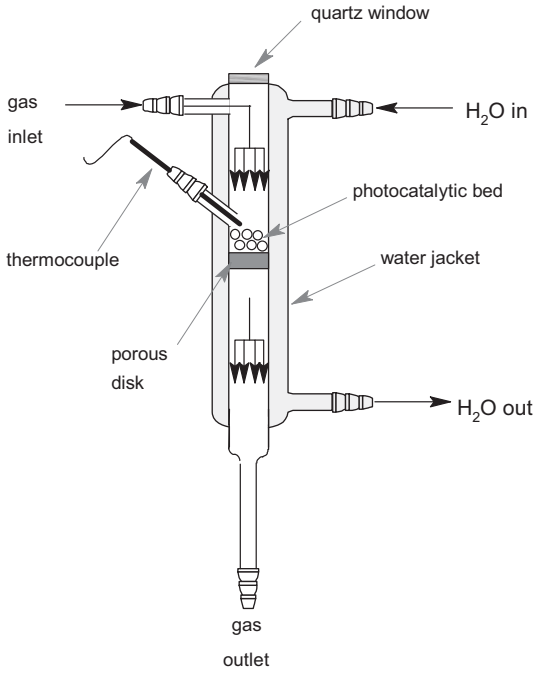

Fig. 4. Photocatalytic fixed bed reactor.

2.4. Photocatalytic oxidation of NO

The apparatus for the photocatalytic study is shown in Fig. 3. 250 ppm of dry NO in nitrogen gas stream was blended with dry air using a gas blender until the appropriate NO concentration was obtained. The gas mixture, at a given flow rate, was used to feed the photocatalytic reactor (Fig. 4). An OSRAM Ultravitalux UVA lamp was used to illuminate the photocatalytic bed in the reactor through the quartz window at the top of the reactor. The distance between lamp and photocatalytic bed was set in order to achieve a constant irradiance of $25 \pm 1\,W\,m^{-2}$ at the catalyst surface. The outlet gas stream was conveyed to a Thermo Environmental 42C chemiluminescence NO–NO_2–NOx gas analyser. A constant temperature of $26.8 \pm 0.14\,^{\circ}C$ was maintained using a water bath circulating water through the external jacket of the reactor.

To study the importance of different levels of adsorbed water, photocatalytic oxidation of NO was monitored using beads as prepared (GB20) and beads having undergone thermal treatment at 110 °C for 1 h (GB110) and at 500 °C for 1 h (GB500) before the NO reaction test. In addition, two *blank* tests were carried out to evaluate the contribution of non-photocatalytic oxidation promoted by UV light and the potential reaction of the NO with water adsorbed on the catalyst surface without irradiation. The first was achieved by introducing the NO/air gas stream in the reactor equipped with TiO_2-free glass beads and the second by leaving the gas stream flowing for about 1 h in the reactor with n-TiO_2 coated glass beads in complete darkness.

3. Results and discussion

3.1. Thermokinetics of TiO_2 surface dehydration

Fig. 5 shows TG analysis and DRIFT spectra as insets. The TG profile (Fig. 5(a)) exhibits a first weight loss step between 20 and 110 °C. DRIFT spectra collected in the same temperature range (inset (b)), show a broad band between 3300 and 3200 cm^{-1}, associated with O–H stretching of molecular H-bonded water and a sharp band at 1623 cm^{-1}, related to *in plane* O–H bending of molecular water. These bands systematically decrease in intensity with increasing temperature and indicate molecular water removal from the TiO_2 surface [23].

A subsequent weight loss step is observed in the range 150–300 °C. Previous works [23,24] show that adsorbed molecular water can still exist at 200 °C and the drop in area for the bands at 3200 and 1623 cm^{-1} in inset (c) confirms this. However, above 150 °C a new band at about 3670 cm^{-1} is formed. This band may be assigned to those surface hydroxyl groups which, being no longer involved in H bonds with molecular water, are now free to vibrate at this frequency. Furthermore, at temperatures higher than 200 °C even chemisorbed molecular water in form of adduct (Eq. (9)) dissociates into *terminal* OH groups (TOH, O–H stretching at 3710 cm^{-1}) and *bridging* OH groups (BOH, O–H stretching at 3660 cm^{-1}) as reported by Trimboli et al. [23] and Henderson et al. [24,25] (Eq. (10)).

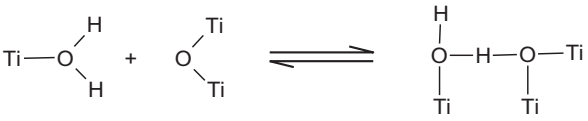

(9)

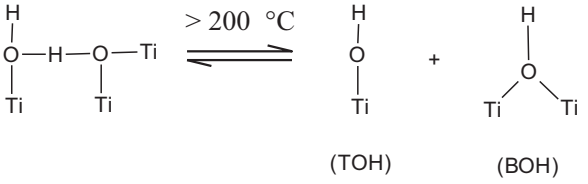

(10)

Inset (d) shows indeed a distinct signal at 3670 cm^{-1} (BOH) with a shoulder around 3719 cm^{-1} (TOH) at a temperature higher than 200 °C. The area of these signals increases in spectra of sample treated at about 350–400 °C (inset (f)) and decreases with further temperature increase suggesting water removal due to TOH and BOH condensation (Eqs. (11), (12) and (13); V_0 is an oxygen vacancy):

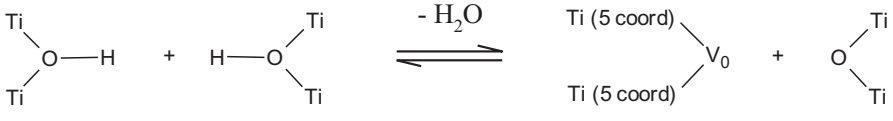

(11)

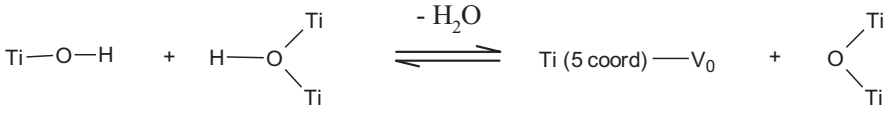

(12)

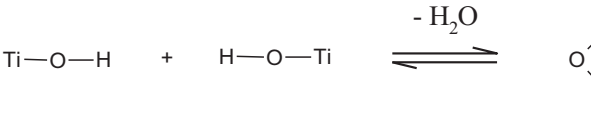

(13)

This contributes to the weight loss measured by TG at temperatures above 350 °C. The continuous weight loss above 200 °C

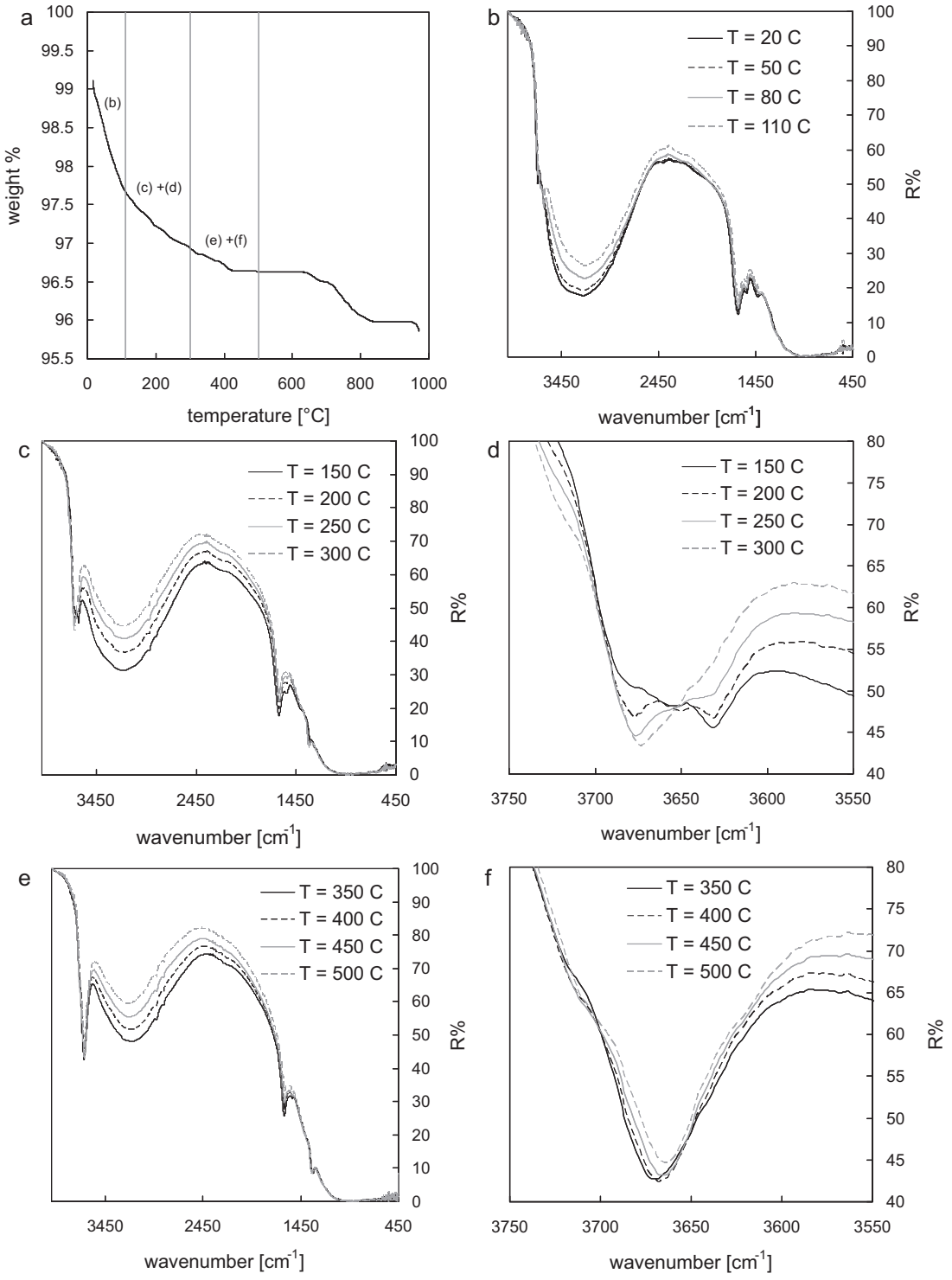

Fig. 5. TG and DRIFT spectra of n-TiO_2 powder.

coupled with the DRIFT signal at 3200 cm^{-1}, which monotonically decreases in area and yet it is present at 500 °C, suggest also a continuous removal of molecular water. However, no molecular physisorbed or H-bonded water can survive these temperatures. Parkins [26] assumed this signal to be associated with strongly chemisorbed water at isolated sites which does not undergo dissociation as highlighted above. The remaining hydration (both molecular water and OH groups) is removed at very high temperature (600–850 °C) as indicated by the TG trend. This confirms once again results previously observed for other metal oxide surfaces [27] regarding the presence of water up to 800–900 °C.

3.2. Overall kinetics of photocatalytic oxidation of NO

Two preliminary *blank* tests (Figs. 6 and 7) indicated no significant NO conversion due to the effect of UV light in the absence of TiO_2 and no reaction with adsorbed species on TiO_2 surface in the darkness, respectively. Pseudo steady state conversions for sample GB20 have been studied at two different gas flow rates, 50

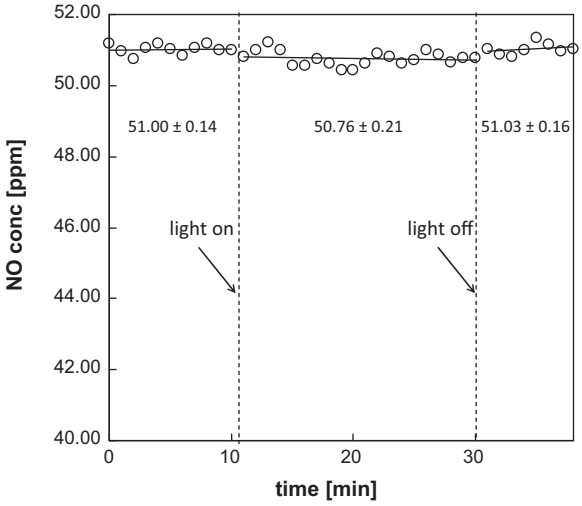

Fig. 6. Effect of photolysis on NO using uncoated glass beads.

and 100 ml min^{-1}, and four different initial NO concentrations, 50, 37, 28 and 25 ppm, to derive kinetic constant and NO adsorption coefficient for assumed Langmuir–Hinshelwood (L–H) kinetics.

The superficial velocity in the reactor, u, and the average gas transit time, τ, can be calculated according to Eqs. (14) and (15):

$$u = \frac{F}{S} \tag{14}$$

$$\tau = \frac{L}{u} \tag{15}$$

where F is the gas flow rate, S the bed cross section, equal to 3.14 cm^2 (2 cm diameter) and L, the illuminated bed depth, equal to 0.2 cm, i.e. the total bed thickness. This assumption is valid since the photocatalytic bed is constituted by TiO_2 coated glass beads and not TiO_2 powder [28,29]. u is then used to derive the axial Peclet number, Pe_a, product of Reynolds number and Schmidt number according to Eq. (16):

$$Pe_a = \frac{uL}{D_e} \equiv Re \cdot Sc \tag{16}$$

where D_e is the diffusion coefficient of NO in air, equal to 0.151 cm^2 s^{-1}.

Table 2 summarizes results obtained for u, τ and Pe_a for the two different flow rates investigated. The Peclet number represents the ratio between convective (uL) and diffusive transport (D_e). In the photocatalytic bed here considered the axial Peclet numbers for both the gas flow rates adopted are below 1, i.e. diffusion prevails over convection. The reactor does *not* have plug flow behaviour: NO concentration profile inside the fixed bed is flat and does not depend on the distance (length of the fixed bed). Therefore it can be treated as a simpler continuous stirred tank reactor or well-mixed reactor (CSTR). Combining the mass balance for a CSTR in Eq. (17):

$$F(C_{NO,in} - C_{NO,out}) = Vr \tag{17}$$

with the L–H kinetics in Eq. (18):

$$\frac{kKC_{NO,out}}{1 + KC_{NO,out}} = r \tag{18}$$

the following expression is derived:

$$\frac{\tau}{C_{NO,in} - C_{NO,out}} = \frac{1}{kKC_{NO,out}} + \frac{1}{k} \tag{19}$$

where r is the reaction rate, $C_{NO,in}$ is the NO concentration at the entrance of the photocatalytic bed and therefore equal to the initial concentration of NO in the gas stream, 50, 37, 28 or 25 ppm, $C_{NO,out}$ is the concentration at the exit of the photocatalytic bed, k the kinetic constant and K the L–H adsorption coefficient. From the linear regression using Eq. (19) (R^2 = 0.998), Fig. 8, and after unit conversion, we observed the following overall constants: $k = 3.00 \times 10^{-4}$ mol m^{-3} s^{-1} and $K = 1.27 \times 10^3$ m^3 mol^{-1}. These values are in good agreement with data already present in the literature [12,18] and provide solid evidence that, with the reactor here used, the photocatalytic oxidation of NO follows the same kinetics already observed by other authors [12,18]. This has been considered as a validation to justify the reliability of our further conversion data.

Table 2
Fix bed reactor fluid dynamic parameters.

Sample	F ml min^{-1}	u cm s^{-1}	τ ms	Pe_a -
GB20	50	0.265	755	0.35
GB20	100	0.531	377	0.70

3.3. Surface hydration, N mass balance and regimes of NO oxidation

Fig. 9 shows the outlet NO, NO_2 and NOx ($C_{NOx} = C_{NO} + C_{NO_2}$) gas phase concentration profiles for n-TiO_2 coated glass beads irradi-

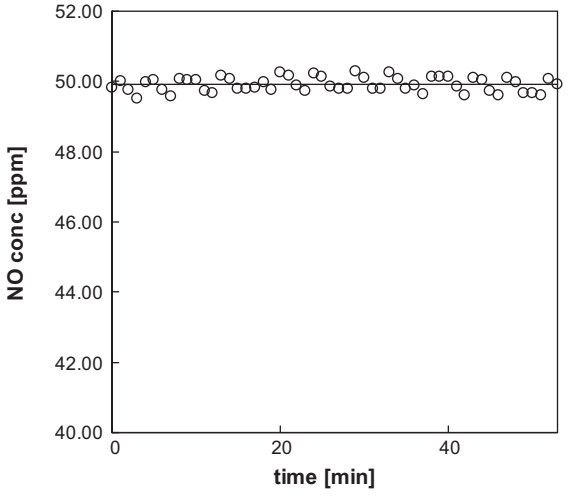

Fig. 7. Effect of the adsorbed water on NO oxidation in the dark.

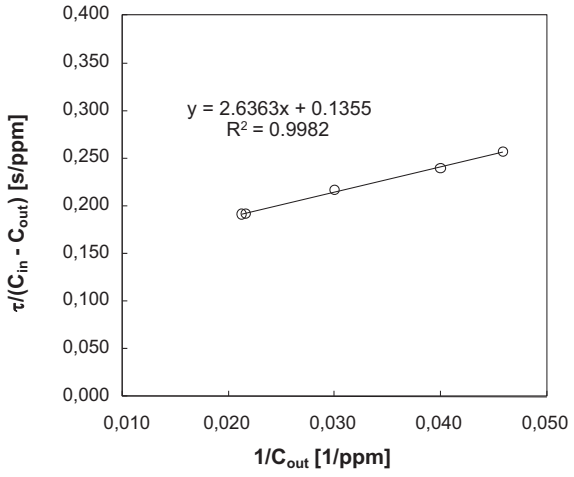

Fig. 8. L–H regression according to Eq. (19).

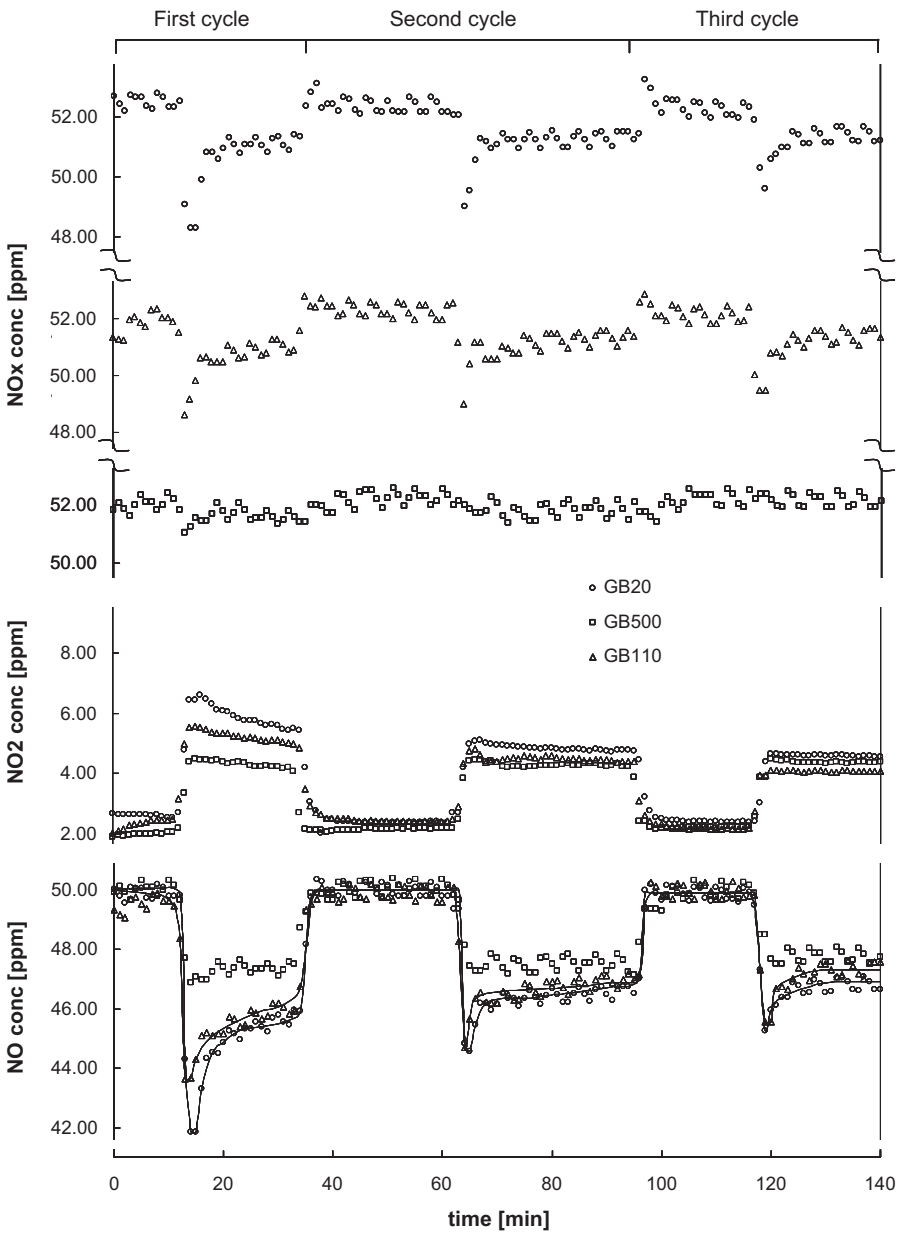

Fig. 9. NO, NO_2 and NOx concentration profiles for $C_{NO,in}$ = 50 ppm and F = 50 ml min^{-1}.

ated with UVA light with an inlet NO/air gas stream at 50 ml min^{-1} and NO concentration equal to 50 ± 0.5 ppm. Three *light on–off* cycles were monitored for each of the three samples.

Before the first cycle, NO gas was flowed through the reactor in the dark until TiO_2 surfaces were saturated (i.e. until $C_{NO,out} = C_{NO,in}$). When light was switched on, the initial drop in NO concentration was 8.2 ppm for GB20, 6.3 ppm for GB110 and 3.1 ppm for GB500, generating a well resolved peak for GB20 and GB110 but a very small one for GB500. This initial NO removal appears to follow the same decreasing trend as is observed for the initial TiO_2 surface hydration as a function of increasing temperature, i.e.: GB20 > GB110 > GB500 (Figs. 5 and 10). NO_2 concentrations achieved a maximum value corresponding with the minimum in NO but do not account for the total NO loss in the gas phase. Indeed the NOx balance showed a drop with peaks similar to the NO profiles. A possible mechanism, consistent with these observations, is shown in Fig. 11. When light is turned on, •OH radicals are formed from the interaction between water and photogenerated positive holes (Eq. (1), donor route) and also via oxygen and photogenerated electrons (Eqs. (3)–(6), acceptor route). This latter route however is kinetically disadvantaged compared to the donor route because the transfer of the photogenerated electron to the adsorbed molecular oxygen is the slowest amongst all of the TiO_2 charge transfer processes (Eqs. (2) and (27) in Table 3). The adsorbed NO reacts very quickly with the adsorbed •OH radicals forming the HONO adduct (Fig. 11). An active site is now vacant and further NO is adsorbed at a higher rate than the conversion of HONO to NO_2. The oxidation of HONO (and/or NO_2^-) to NO_2 (at this early stage in the cycle considered slower than NO adsorption) depends also on the content of water since the initial NO_2 formation follows the same decreasing trends as surface hydration, i.e.: $C_{NO_2,GB20}$ = 6.59 ppm > $C_{NO_2,GB110}$ = 5.53 ppm > $C_{NO_2,GB500}$ = 4.50 ppm.

The proposed mechanism of a fast NO reactive *photoadsorption* and a slower initial conversion to NO_2 is consistent with: (i) the dependency of the area of the adsorption peaks (Fig. 9) on the extent of surface hydroxylation (molecular and dissociated surface

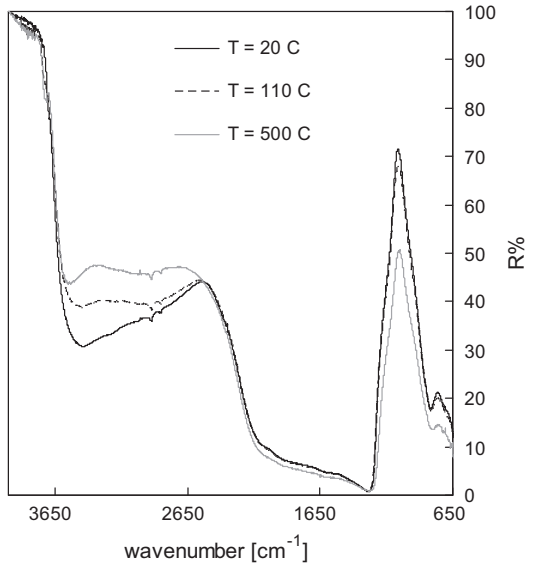

Fig. 10. DRIFT spectra of n-TiO_2 coated glass beads at 20 °C, 110 °C and 500 °C.

Table 3
Primary processes and associated characteristic time domains in the TiO_2-sensitized photoreactions [30]. (*) Characteristic time for this reaction refers to organic molecules only. No data available for NO.

Primary process	Equation	Characteristic time
Charge carrier generation		
$TiO_2 + h\nu \rightarrow h^+ + e^-$	(20)	fs (very fast)
Charge carrier trapping		
$h^+ + Ti^{IV}OH \rightarrow \{Ti^{IV}OH^\bullet\}^+$	(21)	10 ns (fast)
$e^- + Ti^{IV}OH \leftrightarrow \{Ti^{III}OH\}$	(22)	100 ps (shallow trap, dynamic equilibrium)
$e^- + Ti^{IV} \rightarrow Ti^{III}$	(23)	10 ns (deep trap)
Charge carrier recombination		
$e^- + \{Ti^{IV}OH^\bullet\}^+ \rightarrow Ti^{IV}OH$	(24)	100 ns (slow)
$h^+ + \{Ti^{III}OH\} \rightarrow Ti^{IV}OH$	(25)	10 ns (fast)
Interfacial charge transfer		
$\{Ti^{IV}OH^\bullet\}^+ + org \rightarrow Ti^{IV}OH + ox\ org$	(26)	100 ns (slow) (*)
$\{Ti^{III}OH\} + O_2 \rightarrow Ti^{IV}OH + O_2^{\bullet-}$	(27)	ms (very slow)

water) exhibited by GB20, GB110 and GB500; (ii) the light-assisted formation of surface •OH radicals through water and light generated positive holes being a very fast process (Eq. (21), Table 3) [30], (iii) the Langmuir–Hinshelwood kinetics used previously and employed by other authors [12,18,31].

Summarizing the entire initial mechanism as single equation, we obtain

$$NO \xrightarrow{fast,\ ^\bullet OH} HONO \xrightarrow{slow,\ ^\bullet OH} NO_2 \quad (28)$$

Eq. (28) coincides with what Devahasdin et al. [12] hypothesised as a general *initial regime* or *fast initial adsorption plus reaction*.

After this initial stage, the NO conversion decreases significantly for GB20 and GB110. GB500 shows only a very small variation. NO_2 concentration in this period of time decreases. This is the typical feature of a transient behaviour where NO conversion to HONO is the rate determining step and NO_2 is an intermediate which is subsequently oxidised. The final product is HNO_3/NO_3^-:

$$NO \xrightarrow{slow,\ ^\bullet OH} HONO \xrightarrow{fast,\ ^\bullet OH} NO_2 \xrightarrow{fast,\ ^\bullet OH} HNO_3 \quad (29)$$

Once again the NO_2 profiles and the NOx balance provide information on the role of surface water. The rate of conversion of NO_2 (slope of the concentration profile) seems to depend again on the amount of •OH radicals, hence water, on the surface since it follows the usual trend GB20 > GB110 > GB500, suggesting also greater amount of nitrates formed for GB20. NOx balance confirms this hypothesis. Throughout the first cycle, NOx balance in the gas phase does not reach the initial value in the dark and the deficit related to the missing N in gas phase, considered equal to the amount of NO_3^- formed and adsorbed on TiO_2 surface, is: 0.41 μmol m^{-2} g^{-1} for GB20, 0.36 μmol m^{-2} g^{-1} for GB110 and 0.16 μmol m^{-2} g^{-1} for GB500.

When light is turned off after the first cycle, the reaction quenches immediately. NO and NO_2 concentrations return to the initial values and NOx balance in the gas phase reaches 100%. The quick character of the initial concentration recovery (experienced also after the second cycle) when light is off is a clear evidence and further proof that photocatalytic oxidation of NO is a radical-based process.

In the second and third cycles light off–on, we note the same observations for cycle 1. When light is turned, a fast NO reactive photoadsorption occurs with generation of NO_2 which approaches the transient period summarized by Eq. (29). However, from cycle to cycle, we can observe that, for GB20 and GB110:

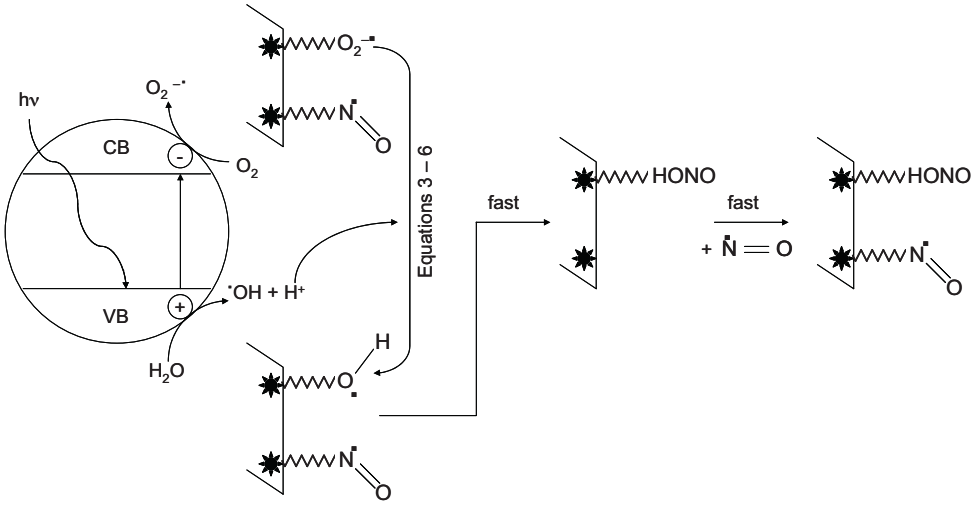

Fig. 11. NO photoadsorption on light activated TiO_2 (* adsorption site; /\/\/\/\/ undefined bond).

(i) the area of the peak related to the initial fast reactive photoadsorption of NO continuously decreases from cycle to cycle;
(ii) NO concentration monotonically increases while NO_2 concentration monotonically decreases; despite the fact that GB20 shows general lower NO concentration and higher NO_2 concentration than GB110 (lower water content), the differences between the two samples become smaller as a function of number of cycles.

For GB500, the much reduced amount of water (molecular and dissociated) on the surface minimises considerably the effects observed for GB20 and GB110. The very small peak of fast reactive photoadsorption of NO experienced in the first cycle disappears completely in the following two. NO and NO_2 concentrations remain quite constant in the second and third cycles with good NOx balance in the gas phase that suggests very low amount of nitrates formed in the first cycle, even less in the second and no measurable nitrates in the third (concentration of total NOx in the gas phase in the dark is equal to that during illumination, i.e., the balance closes to 100% with NO and NO_2 only).

This evidence is likely to be attributed to *deactivation* of the reactive surface by means of: water consumption during the reaction (which is not continuously supplied through the gas feed) and *irreversible adsorption* of nitrates which reduces the number of available adsorption sites.

Integration of the gaps in the NOx balance can provide a quantitative view of the deactivation phenomena described above. Fig. 12 shows the progressive reduction of specific surface area for the three batches due to nitrate formation, under the assumptions that: (i) all the NOx missing in the gas phase can be accounted for as NO_3^- formation; (ii) NO_3^- does not desorb from the TiO_2 surface; (iii) the average radius of NO_3^- is 1.96 Å [32]. According to quantitative data shown in Fig. 12, the deactivation of active sites due to adsorbed nitrates and consequent reduction in available surface area is occurring but the amount of available surface area is significantly still very high after a total illumination period of about 80 min. Therefore in this period of time, the consumption of water (molecular and dissociated) in the reaction might play a major role in the overall deactivation. The apparent absence of nitrate formation observed for GB500 in the third cycle is not completely understood yet, however different hypothesis may be provided. Devahasdin et al. [12] observed no nitrate formation with NO_2 as the final oxidation product once all the sites responsible for NO_3^- formation are irreversibly occupied. Although this is likely to be the case after many hours of

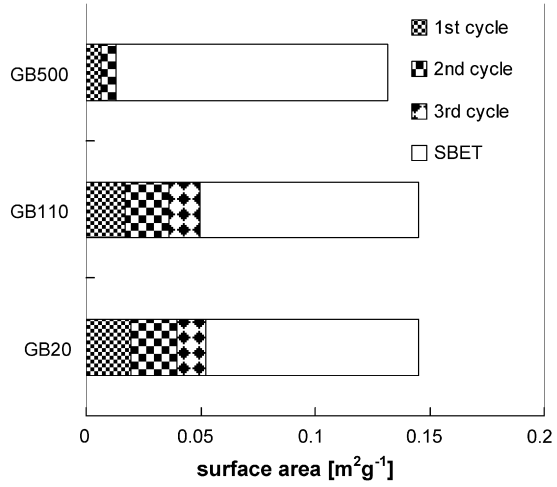

Fig. 12. Surface area loss due to NO_3^- formation and adsorption compared to the total BET specific surface area (data referred to the TiO_2-coated glass beads).

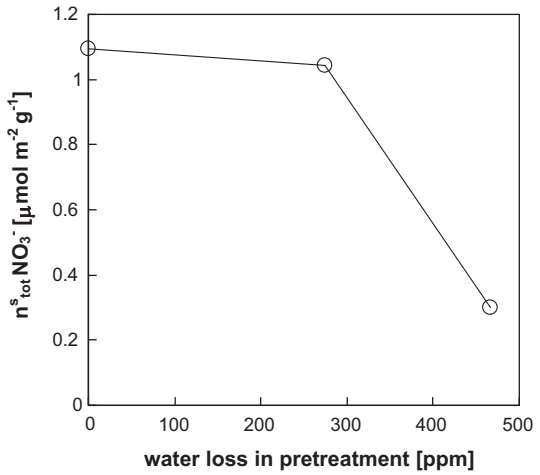

Fig. 13. Effect of initial water content on total moles of NO_3^- formed on TiO_2 surface.

activity, in our conditions the available surface area is still high and it is difficult to reconcile this behaviour with occlusion of all the active sites. We propose alternatively (on the pure basis of our results) that oxidation to nitrate is inhibited by the low availability of surface water, allowing oxidation of NO only to NO_2 and not further. However we are aware that Hashimoto et al. [31] detected nitrate formation due to solely effect of $O_2^{-\bullet}$ but the degree of surface hydration was not defined. One must however consider the relative impact of the water mediated (hydroxyl radicals) and $O_2^{-\bullet}$ mediated oxidation processes, given the information provided in Table 3 on reaction rates.

Data obtained by integration of the areas related to the NOx balance can also be used to plot the total amount of NOx lost from the gas phase (considered equal to the total amount of NO_3^- formed) over the three cycles versus the water loss due to the pre-treatment that GB110 and GB500 experienced (Fig. 13). Even though more data points are necessary to identify a better trend, Fig. 13 suggests that, although the absolute amount of water lost between GB20 and GB110 is similar to the amount lost between GB110 and GB500, the total number of moles of NO_3^- produced by the latter is significantly lower. The reason might be found in the nature of water removed. DRIFT spectra showed that between 20 °C and 110 °C, H-bonded molecular water is removed; between 110 °C and 500 °C it is chemisorbed water (molecular and dissociated) which leaves the surface. Fig. 13 therefore highlights that in the photocatalytic formation of NO_3^-, chemisorbed water is much more active than H-bonded molecular water. This can be considered as further experimental justification for the use of a Langmuir–Hinshelwood kinetics model.

3.4. O_2 radicals-based oxidation and synergistic effect of the couple H_2O–O_2

As already mentioned, Hashimoto et al. [31] proved that NO can also be oxidised, on light irradiated TiO_2 surfaces, by superoxide radicals, $O_2^{-\bullet}$ (Eq. (2)). Their assumption is supported by infrared spectra showing typical NO_3^- vibration modes on the surface of UV irradiated titania in the presence of oxygen and NO, together with EPR spectra that, after revealing increase of $O_2^{-\bullet}$ radicals adsorbed on the surface of UV irradiated titania in the presence of oxygen, showed drop in spectrum intensity related to $O_2^{-\bullet}$ simultaneously to NO exposure. Although our analysis focused on the effect of surface water and data do not allow us to discriminate the contribution attributed only to adsorbed oxygen, this extra oxidation route through superoxide species *must be active under our conditions as well* and therefore contribute to the overall NO conversion. Since

the generation of •OH radicals from molecular oxygen depends on the amount of water present (synergistic effect of H_2O–O_2): O_2 needs the protons exchanged by the reaction of water with positive holes (Eq. (3)); NO photocatalytic oxidation under conditions of water deficiency (GB500) might be characterised by a larger contribution of the O_2 radicals-based route. This idea seems to fit quite well with the flat NO and NO_2 concentration profiles measured for GB500.

Finally, independently of the actual oxidising species that H_2O and O_2 produce, their coupling is necessary to sustain the activation of the photocatalyst since they are responsible for trapping and/or transferring the photogenerated charge carriers (conductance band electrons and valence band positive holes) that would otherwise promptly recombine. Significant removal of one of the two species (like in our case comparing GB20 with GB500) can therefore decrease the overall activity due to much higher levels of electron–hole recombination.

4. Conclusions

This study has linked photocatalytic performances for nitric oxide, NO, oxidation in a continuous fixed bed reactor to the state of water adsorbed on TiO_2 surface. A kinetic study using an assumed Langmuir–Hinshelwood model allowed an overall kinetic constant and a NO adsorption coefficient to be determined which are in good agreement with previous findings [12,18]. Conversion data coupled with DRIFT investigations on the surface of the three batches examined, GB20, GB110 and GB500, showed a significant drop in overall activity when, by thermal treatment, chemisorbed molecular and dissociated water is removed. The PCO of NO is assumed to go through an initial stage of fast NO reactive photoadsorption with formation of NO_2 which approaches a transition stage (and later on a pseudo steady state) where NO_2 is converted to NO_3^-. All the steps from NO to NO_3^- in the regimes observed have been found to be •OH radical-dependent, hence water content-dependent. Water consumption on the TiO_2 surface (if not continuously supplied) and adsorbed NO_3^- species may be considered as the main factors for catalyst deactivation. Further spectroscopic surface studies on the light irradiated TiO_2 surface during the PCO reaction may be the subject of a future study and may be useful to completely identify and clarify the deactivation phenomena here observed.

Acknowledgements

The authors are grateful to the European Community under the Marie Curie Research Training Network MRTN-CT-2005-019283 “Fundamental understanding of cementitious materials for improved chemical physical and aesthetic performance” (http://www.nanocem.org/MC-RTN/) for the full support of Andrea Folli.

References

[1] R.M. Harrison, Pollution: Causes, Effects and Control, 2, The Royal Society of Chemistry, Cambridge, 1992.
[2] D. Elsom, Atmospheric Pollution, 1, Basil Blackwell, New York, 1987.
[3] J.H. Seinfeld, Atmospheric Chemistry and Physics: From Air Pollution to Climate Change, 1, Wiley, New York, 1998.
[4] F.A. Cotton, G. Wilkinson, Advanced Inorganic Chemistry, 5, Wiley-Interscience, USA, 1988.
[5] C.A. Latta, Plant Eng. 52 (1998) 105–112.
[6] S.K. Gangwal, G.B. Howe, J.J. Spivey, P.L. Silveston, R.R. Hudgins, J.G. Metzinger, Environ. Prog. 12 (1993) 128.
[7] C. Hogue, EPA assesses state of nation’s outdoor air, Chem. Eng. News 78 (2000) 5–6.
[8] L. Cassar, P. Baglioni, International RILEM Symposium on Photocatalysis, Environment and Construction Materials, RILEM, Florence, 2007.
[9] D.H. Chen, K. Li, Photocatalytic Coating on Road Pavements/Structures for NOx Abatement, Lamar University, Beaumont, 2007.
[10] S. Chen, G. Cao, Study on the photocatalytic oxidation of NO_2^- ions using TiO_2 beads as a photocatalyst, Desalination 194 (2006) 127–134.
[11] J.S. Dalton, P.A. Janes, N.G. Jones, J.A. Nicholson, K.R. Hallam, G.C. Allen, Photocatalytic oxidation of NOx gases using TiO_2: a surface spectroscopic approach, Environ. Pollut. 120 (2002) 415–422.
[12] S. Devahasdin, C.J. Fan, K. Li, D.H. Chen, TiO_2 photocatalytic oxidation of nitric oxide: transient behavior and reaction kinetics, J. Photochem. Photobiol. A: Chem. 156 (2003) 161–170.
[13] H. Ichiura, T. Kitaoka, H. Tanaka, Photocatalytic oxidation of NOx using composite sheets containing TiO_2 and a metal compound, Chemosphere 51 (2003) 855–860.
[14] A. Mills, S. Le Hunte, An overview of semiconductor photocatalysis, J. Photochem. Photobiol. A: Chem. 108 (1997) 1–35.
[15] D. Ollis, H. Al-Ekabi, Photocatalytic purification and treatment of water and air, Elsevier, New York, 1993.
[16] C.S. Poon, E. Cheung, NO removal efficiency of photocatalytic paving blocks prepared with recycled materials, Constr. Build. Mater. 21 (2006) 1746–1753.
[17] UNI_11247, Determination of the Degradation of Nitrogen Oxides in the Air by Inorganic Photocatalytic Materials: Continuous Flow Test Method, 2009, pp. 1–11.
[18] H. Wang, Z. Wu, W. Zhao, B. Guan, Photocatalytic oxidation of nitrogen oxides using TiO_2 loading on woven glass fabric, Chemosphere 66 (2007) 185–190.
[19] J. Zhao, X. Yang, Photocatalytic oxidation for indoor air purification: a literature review, Build. Environ. 38 (2003) 645–654.
[20] A. Fujishima, K. Hashimoto, T. Watanabe, TiO_2 Photocatalysis: Fundamentals and Application, 1, BKC, Tokyo, 1999.
[21] A. Folli, U.H. Jakobsen, G.L. Guerrini, D.E. Macphee, Rhodamine B discolouration on TiO_2 in the cement environment: a look at fundamental aspects of the self-cleaning effect in concretes, J. Adv. Oxid. Technol. 12 (2009) 126–133.
[22] N. Daneshvar, D. Salari, A. Niaei, M.H. Rasoulifard, A.R. Khataee, Immobilisation of TiO_2 nanopowder on glass beads for the photocatalytic decolorization of an azo dye C.I. direct red 23, J. Environ. Sci. Health 40 (2005) 1605–1617.
[23] J. Trimboli, M. Mottern, H. Verweij, P.K. Dutta, Interaction of water with titania: implications for high-temperature gas sensing, J. Phys. Chem. B 110 (2006) 5647–5654.
[24] M.A. Henderson, Structural sensitivity in the dissociation of water on TiO_2 single-crystal surfaces, Langmuir 12 (1996) 5093–5098.
[25] M.A. Henderson, W.S. Epling, C.H.F. Peden, C.L. Perkins, Insights into photoexcited electron scavenging processes on TiO_2 obtained from studies of the reaction of O_2 with OH groups adsorbed at electronic defects on TiO_2(1 1 0), J. Phys. Chem. B 107 (2002) 534–545.
[26] N.D. Parkyns, in: P. Hepple (Ed.), Chemisorption and Catalysis, Elsevier, London, 1970, pp. 150–171.
[27] S. Ek, A. Root, M. Peussa, L. Niinistö, Determination of the hydroxyl group content in silica by thermogravimetry and a comparison with 1H MAS NMR results, Thermochim. Acta 379 (2001) 201–212.
[28] D.F. Ollis, Photocatalytic powder layer reactor: a uniformly mixed gas phase occurring in a catalytic fixed-bed flow reactor, Ind. Eng. Chem. Res. 41 (2002) 6409–6412.
[29] A. Chen, G. Lu, Y. Tao, Z. Dai, H. Gu, Novel photocatalyst immobilised on springs and packed photoreactor, Mater. Phys. Mech. 4 (2001) 121–124.
[30] M.R. Hoffmann, S.T. Martin, W. Choi, D.W. Bahnemann, Environmental applications of semiconductor photocatalysis, Chem. Rev. 95 (1995) 69–96.
[31] K. Hashimoto, K. Wasada, N. Toukai, H. Kominami, Y. Kera, Photocatalytic oxidation of nitrogen monoxide over titanium(IV) oxide nanocrystals large size areas, J. Photochem. Photobiol. A: Chem. 136 (2000) 103–109.
[32] W.L. Masterton, D. Bolocofsky, T.P. Lee, Ionic radii from scaled particle theory of the salt effect, J. Phys. Chem. 75 (1971) 2809–2815.